Journal of Imaging Science and Technology® 52(3): 030508–030508-9, 2008.

Dedicated Image Analysis Software Tool for the Evaluation of the Resorption Activity of Cultured Osteoclasts

Stefano Z. M. Brianza and Patrizia D'Amelio
Department of Internal Medicine, University of Torino, Corso Dogliotti 14, 10126 Torino, Italy
E-mail: stefanobrianza@yahoo.it

Marco Cerrato and Cristina Bignardi
Department of Mechanics, Politecnico of Torino, Corso Duca degli Abruzzi, 24, 10129 Torino, Italy

Anastasia Grimaldi
Department of Internal Medicine, University of Torino, Corso Dogliotti 14, 10126 Torino, Italy

Gian P. Pescarmona
Department of Medical Oncology Center on Experimental Medicine (CeRMS), University of Torino, Via Santena 5 bis, 10126 Torino, Italy

Giancarlo Isaia
Department of Internal Medicine, University of Torino, Corso Dogliotti 14, 10126 Torino, Italy

Abstract. *A semi-automated image analyzing system was developed for the quantitative study of the in vitro osteoclast activity. It is able to determine the percentage of the matrix reabsorbed by cultured osteoclasts. It counts and sizes the worn areas and displays the results together with two-color coding useful for visual interpretation. A specific semi-automated procedure was designed to simulate human sight. It detects local gray level differences while matching with the surrounding gray levels. It implements routine calculation enabling the operator to continuously control the process. We were able to accurately and precisely quantify the reabsorbed percentage of meaningful fields in a slice. This image-analyzing system is useful in the study of physiological or pathological osteoclast activity, in various diseases involving bone, such as osteoporosis, Paget's disease of bone or neoplastic conditions, and in the evaluation of osteoclast response to various agents. © 2008 Society for Imaging Science and Technology.*
[DOI: 10.2352/J.ImagingSci.Technol.(2008)52:3(030508)]

INTRODUCTION

Bone resorption is carried out by osteoclasts (OCs) that are multinucleated cells formed by the fusion of marrow-derived cells.[1,2] An imbalance between bone formation and bone resorption, with an increase in OC number and/or activity, is thought to underlie the pathogenesis of a lot of bone diseases; for example, metabolic, such as osteoporosis,[3,4] and metaplastic, such as Paget's disease of bone,[5] but also the pathogenesis of bone metastasis.[6,7] Hence, the assessment of OCs' formation and activity and their response to pharmaceutical agents is of central importance to understand the physiopathological processes involved in bone metabolism.

Received Sep. 14, 2007; accepted for publication Feb. 25, 2008; published online May 19, 2008.
1062-3701/2008/52(3)/030508/9/$20.00.

In vitro OCs capability in reabsorbing bone can be evaluated measuring biochemical markers released in the culture medium or visually quantifying the portion of matrix eroded by cells. The *in vitro* nowadays golden standard used to define the osteoclast function is their resorption capability. The cortical bone slices, the dentine slices, and the submicrometer synthetic calcium phosphate thin films are actually the most used cell culture techniques to study osteoclasts.[6–12]

The quantification of resorption capability relies mostly upon two-dimensional analysis of resorption pits of variable depth based on optical methods. The slices can be examined by light microscopy and the total area of resorption visually estimated. Matrix resorption can be detected by the change in light transmission due to the mutated thickness. Stereo mapping of the resorption volume is also performed on bone or dentine slices that exhibit complex irregular three-dimensional resorption pits of no fixed depth.[11,13] This time consuming technique is needless using the submicrometer synthetic calcium phosphate thin films due to their controlled thickness. As the film is thin and of uniform thickness, the amount of material removed can be related to the plan area of the created voids. As regards the submicrometer synthetic calcium phosphate thin films one of the manufacturing firms (Becton Dickinson and Co., Franklin Lakes, NJ, USA) provides a customer service that stains the Osteologic Biocoated device with a routine histological fixative to demonstrate the presence of calcium phosphate. The calcium specific stain is taken up only in those areas where the film is intact and the stain content measured by a custom analyzer. Time consuming manual drawing of the reabsorbed areas using an eyepiece reticule and reflected light microscopy is

also reported.[14] This technique leads inevitably to inaccurate and imprecise results.

The bone research community has not adopted a specific standard method to analyze pit formation assays. The purpose of our work was to develop an accurate and precise tool in support to bone researchers. Emulating the human vision, it detects local gray level differences while matching with the surrounding gray levels.

MATERIAL AND METHODS

The aim of the different procedures of image analysis applied here was the detection of the areas reabsorbed by the osteoclast activity and their quantitative characterization. The reabsorbed areas are defined as the areas where the matrix lost its original pattern. The operator is requested to take pictures of fields of interest in the slices he/she his willing to analyze in photo sessions, to acquire these pictures with a personal computer, and to enter and control the image analysis chain. The technique was developed to primary examine pictures of bone slices, dentine slices and the multiwell BD BioCoat™ Osteologic™ Bone Cell Culture System (Becton Dickinson and Co., Franklin Lakes, NJ, USA), but the algorithm can be virtually applied on pictures of other thin mediums. Usually osteoclast or their precursors are cultured on these mediums and, at the end of the culture period, the adherent cells are removed in order to show the bare surface that can be analyzed. Using the multiwell BD BioCoat™ no staining is required, while using dentine or bone slices a staining with toluidine blue is required.

Photo Session

A photo session is defined as a sequence of pictures of matrices properly treated where the setup of the microscope is fixed. In order to get a usable image, the specimen must be properly illuminated and the light path of the microscope properly set up. The Köhler illumination is the suggested setup for proper image generation.[15] Fields of interest have to be pictured with a standard digital camera attached to a common inverted research microscope. For each photo session, the operator is primarily requested to perform brightness and space calibration. A picture of an empty well plate of the same thickness of the matrix coated ones, illuminated as for usual readings, is required for the brightness calibration. A picture of a slice ruler is required for the space calibration. Required picture format is the common JPEG (lossy or lossless), 1536×2048 pixels, 24 bits per pixel (16×10^6 colors).

Image Acquisition, Storage, and System Requirements

By means of an adequate coupling (USB connection, usually) pictures of the photo sessions can be forwarded to a computer hard disk, saved in folders and analyzed at any time. The software, which runs on the Windows platform, was written in Visual Basic® 6 and uses FreeImage libraries. Minimum system requirements are a Pentium® IV (CPU 2.66 GHz and RAM 512 MB) or compatible. An additional framegrabber card is required.

The Image Analysis Chain

The image analysis chain starts as an operator loads the software (flow chart shown in Figure 1). Explicit messages on the video drive the operator throughout the entire process. Message boxes allow operators to choose over the entire analysis for different options and enable only the controls relative to their choices. To detect the reabsorbed areas in a highly complex image context, we employed different operations and steps of processing images: brightness and length calibration, picture correction, threshold selection, picture scanning in three steps, and macroscopic corruptions erasing. These operations are intended for pictures taken in the same photo session. Results achieved with pictures coming from different photo sessions, using different brightness and space pictures for calibration, may be inaccurate. As the operator selects the JPEG picture to analyze, an identical copy of the picture is automatically saved to the computer's hard drive in Bitmap (.bmp), 8 bits per pixel format. The entire process will operate on this copy, leaving the original picture unmodified. In order to enhance the readability of the pictures and to speed up the procedure as the copy is automatically reloaded and displayed on video, gamma and contrast corrections are applied, and it is downsized to 1024×768 pixels by means of FreeImage (Floris van den Berg) functions. FreeImage is a free and open source graphics library for Windows®, Linux, and Mac OS. An advanced parameterized scaling filter, Mitchell and Netravali's bicubic filter, is used to downsize the pictures. It uses a cubic function to produce very smooth output while maintaining dynamic range and sharpness.

Brightness and Length Calibrations

The aim of these procedures, operator selected, is to correct for eventual inhomogeneous slice lighting and to dimension the observed slice features. A suitable tool detects pixel-by-pixel light distribution, ranging from H000000 (black) to HFFFFFF (white), on the picture of the empty slice. The reciprocal of the value detected for each pixel, raised to the fifth power, is saved as an adjustment value in a 1024×768 pixel matrix. In order to avoid division by zero, when the H000000 value is found, it is substituted with H000001. This matrix, here defined as the natural matrix (N), is saved on the hard disk in a data file.

In order to further reduce the effects of an eventual inaccurate Köhler illumination, another 1024×768 pixel matrix, here defined as artificial matrix (Art), is enclosed as a data file in the software package. This fixed set of data was created reading through the same calibration tool as for an empty picture, 1024×768 pixels, 8 bit per pixel, created by Photoshop® 6.0, distinguished by a light central overexposure.

The space calibration can be performed as usual by drawing a line of known length on the suitable picture of a slice ruler and determining the pixels' length ratio. These ram-stored values will be used for all the pictures belonging to the same photo session, speeding up the procedure. (They also stay on the hard disk until expressly replaced with other

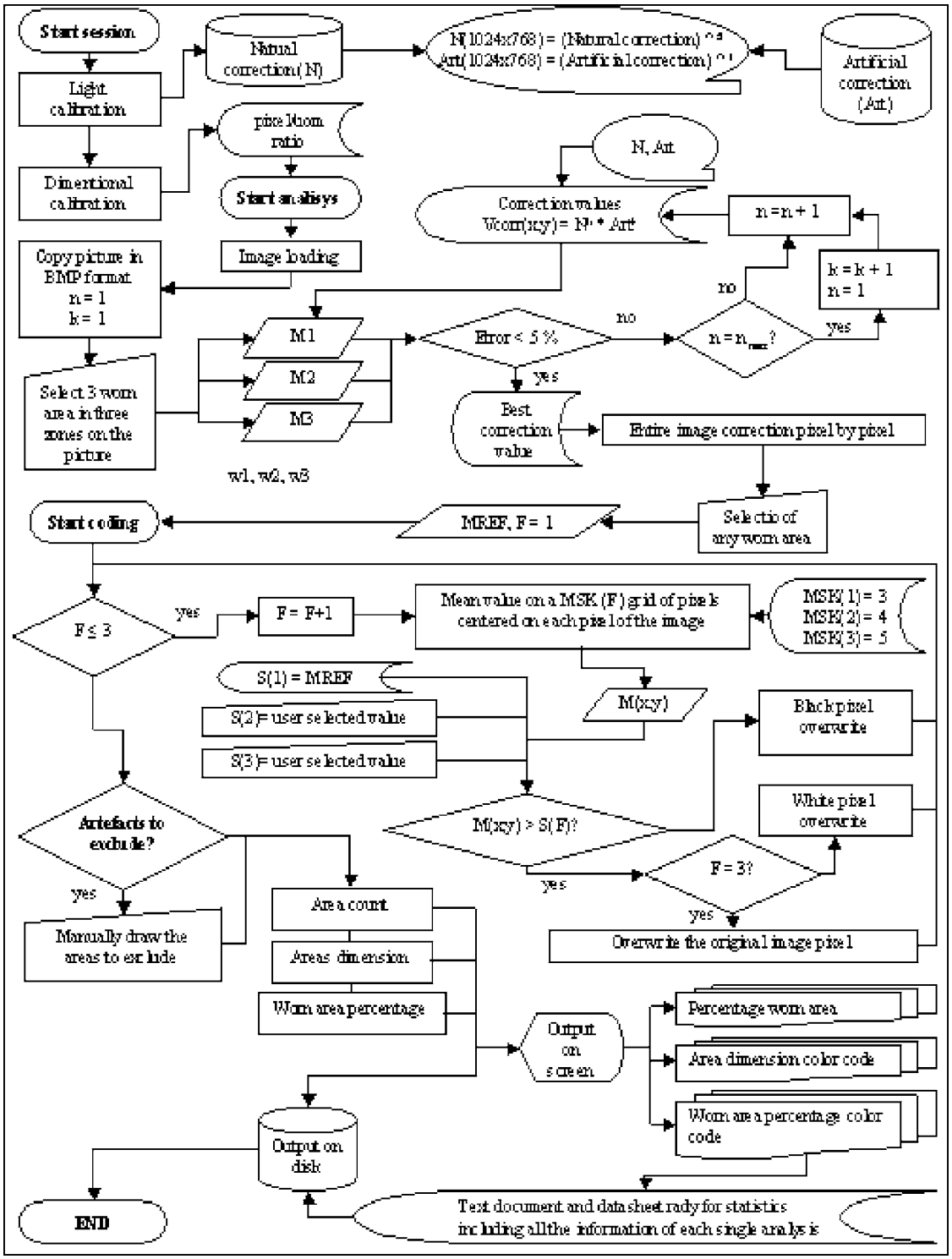

Figure 1. Flow-chart of the image analysis chain.

calibrations.) During the analysis of a photo session it is not required to repeat the calibration.

Picture Correction

Led by unequivocal messages the operator is requested to select with the mouse pointer three points in three areas recognized as reabsorbed (for calcium phosphate films) or not reabsorbed (for bone and dentine slices), respectively, in the central, intermediate, and peripheral parts of the loaded picture (Figure 2, top panels). They match areas roughly evenly lightened at similar radial distances from the center of the picture. With the pointer, he/she defines three local mean brightness values, here defined as M1, M2, and M3. These are the mean values of the brightness of three grids, R1, R2, R3, of 7×7 pixels, surrounding the selected ones. If the three means range beyond 5% a procedure aimed to bring them back into that range starts. This procedure alters

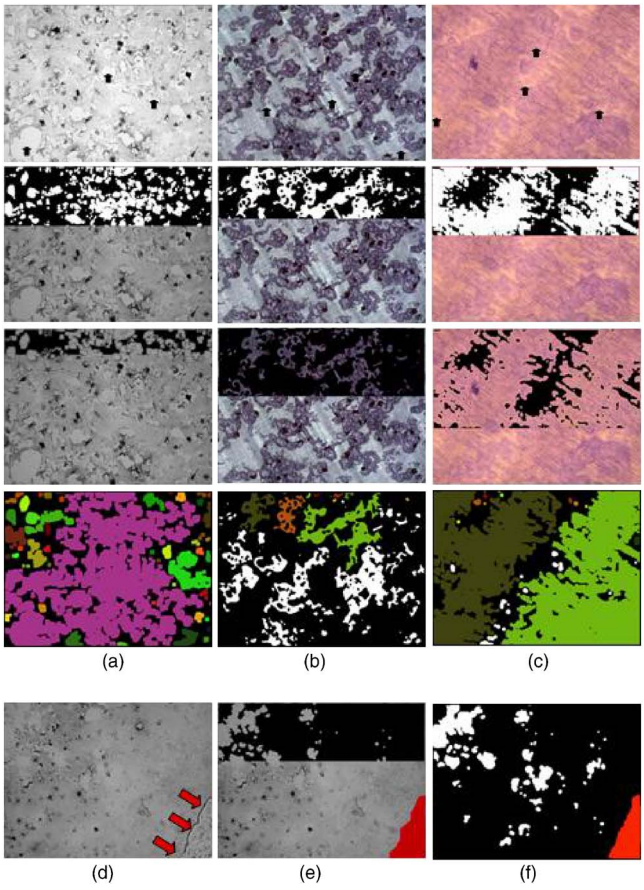

Figure 2. Analysis of pictures of an osteologic biocoated (a), of a bone slice (b) and of a dentine slice (c). The top panels are the pictures properly converted in Bitmap format, corrected and downsized as the software loads them and ready to enter image analysis chain. In the bottom panels are the same pictures at the end of the third step of picture scanning: the original picture as background allows the operator to clearly gauge the accuracy of the image treatment. The black arrows indicate the areas selected by the operator at the beginning of the procedure: for osteologic biocoated, it is requested to select pits in the central, intermediate, and peripheral zones of the picture; for dentine and bone slices, it is requested to select non-eroded surfaces in the central, median, and external zones of the picture and then the center of a pit. Panels (d), (e), and (f) are examples of how the software is able to exclude artifacts. Panel (d) shows the picture of an osteologic biocoated with the edge of the slice included (red arrows). Panel (e) shows how the operator can exclude the artifact from the analysis. Panel (f) shows the analysis completed with the eroded areas recognized and the artifact colored in red.

nonlinearly the calculation of the three means: it corrects M1, M2, and M3, applying pixel-per-pixel to the grids R1, R2, and R3, the product of the matrix N and Art, element-per-element, raised, respectively, to two different exponents, n and k. Two cycles linearly raise n and k. In order to maximize the effect of the natural matrix N with respect to that of the artificial Art, the exponents are stepped up so that for a unit increase of k, n is continuously increased to its maximum and then resets its minimum. Since data inside the matrixes are the inverse of the brightness, exponential enhancement has basically the effect of flattening the grid surfaces and thus moves the data nearer the three means Me1, Me2, and Me3. If the exponent k reaches its maximum and the three means still range beyond 5% the procedure is stopped. The operator is then able to restart the picture correction procedure or to abort the analysis. Once the deviation is under 5% the optimal correction value determined is applied to the entire picture, pixel-by-pixel, to obtain a corrected image.

Threshold Selection

A message invites then the operator to pick another reabsorbed area anywhere on the corrected image. Thereby, he/she defines a reference threshold, here defined as MREF, the software will use to scan the entire picture. The threshold is again the mean value of brightness of a grid of 7×7 pixels around the selected one.

Picture Scanning

First step. The aim of the first step is to discern the worn areas from the matrix and to exclude smaller artifacts. Smaller artifacts are defined as cell remnants on worn areas and irregular matrix patterns with bright spots. The software automatically starts to read the picture. The graphical results of routine calculations are continuously plotted on the original picture under the operator's continuous audit. Pixel by pixel, the picture is scanned by lines and the local mean brightness value, here defined as $M1(x,y)$, of a 7×7 grid of pixels around the examined one, here defined as pixel(x,y), is calculated. If the local mean brightness value $M1(x,y)$ is lower than the threshold MREF, the considered pixel(x,y) is believed to be part of the matrix of a worn area. The pixels assessed to be part of the matrix are plotted black; otherwise they are plotted white. The operator gauges in real time the accuracy of the software routine calculations appraising the coherence of the refreshing new image, made of black and white pixels, with respect to the original one (Fig. 2, second line panels). During the refresh, if not satisfied, the operator can adjust the developing graphical results using an on-screen slider able to alter the threshold in real time. The developing image of the first step is RAM stored in a matrix 1024×768 pixels, 8 bits per pixel, here defined as M1. At the end of the reading a message box asks the operator to accept or reject the result of the first step. On rejection, the matrix M1 is overwritten by repeating the first step. On acceptance the matrix M1 becomes the virtual image to be scanned in the next step.

Second step. The aim of the second step is to roughly refine the edge of the worn areas and to exclude larger artifacts. The software automatically re-plots the original picture and starts to read the virtual image, composed by the matrix M1, made of black and white pixels. The graphical results of the new routine calculations on M1 are plotted again on the original picture under the operator's continuous audit. Pixel-by-pixel the picture M1 is scanned by lines and the local mean brightness value, here defined as $M2(x,y)$, of a 9×9 grid of pixels around the examined one, the pixel(x,y), is calculated. If the local mean brightness value, $M(x,y)$, is lower than a threshold, here defined as $M2_{temp}$, the considered pixel(x,y) is believed to be part of the matrix of a worn area. The operator determines the threshold $M2_{temp}$ continuously, using the on-screen slider. The slider is able to select a gray scale value such as to cover all the possible

combinations of black and white pixels in a 9×9 grid. The effect is a control on the edge of the worn areas and the exclusion of artifacts. The pixels assessed to be part of the matrix are plotted black otherwise white and RAM stored in a matrix 1024×768 pixel, 8 bits per pixel, here defined as M2. The operator gauges in real time the accuracy of the software's routine calculations, appraising the coherence of the refreshing new image with respect to the original one at the end of each step. At the end of the reading, a message box asks the operator to accept or reject the result of the second step. On rejection, the matrix M2 is overwritten by repeating the second step. On acceptance the matrix M2 becomes the virtual image to be scanned in the following step.

Third step. The aim of the third step is to increase the refinement of the edge of the worn areas and to exclude larger artifacts. It works exactly as the second step but operates with a matrix 11×11 and plots on video only the black pixels. As the pixel assessed remains transparent as part of the worn areas, the operator has the opportunity to clearly gauge the accuracy of the image treatment (Fig. 2, third line panels). At the end of the reading a message box asks the operator to accept or reject the result of this step. On rejection the matrix M3 is overwritten repeating the third step. On acceptance, the matrix M3 becomes the virtual image to be analyzed in the next steps. (Owing to the architecture of our scanning procedure, at the end of the third step a strip of five pixels for each side is lost.)

Erasing Macroscopic Corruptions

Once the third reading is accepted, a message box asks operators if they are willing to erase areas of macroscopic corruption. Those are defined as areas that are indecipherable or damaged by the operator seeding the culture. The operators thus have the opportunity to draw with the mouse pointer on the original picture the edge of the parts they considers to be corrupted. An automatic function creates an area inside each closed edge. The pixels recognized to be part of a corrupted area are plotted red and RAM stored in a matrix 1024×768 pixels, 8 bits per pixel, here defined as M_{er}. Superimposing the matrix M_{er} on the matrix M3, a definitive matrix M_{def} is written, plotted, and forwarded to the calculations[(Fig. 2, panels (d,e,f]).

Calculations

The program recognizes, counts, and sizes the reabsorbed areas. Their sum is expressed as a percentage of the entire scanned area and a graph frequency-dimension is plotted. A first color coding links the reabsorbed percentage to a color from blue to yellow and assign it to the whole areas recognized as reabsorbed (Fig. 2, fourth line panels). A second links a color from blue to yellow to the worn area size and the entire picture size ratio and assigns it area by area. Numerical results are saved in two separate text files and the resulting pictures are saved in JPEG format. Such system is configured to link with a computerized datasheet ready for statistical analysis of the resulting data.

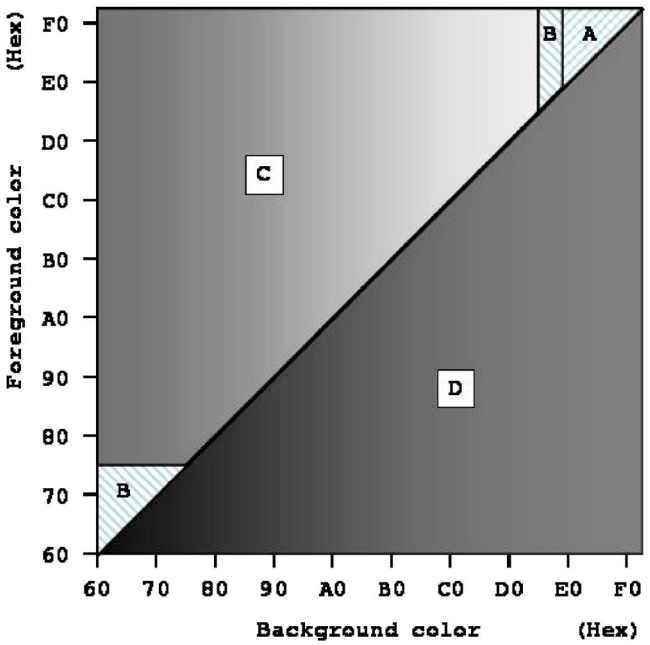

Figure 3. Schematic grayscale combinations of colors for the matrix (D) and worn areas (C). In a reasonable range of light exposures, for a given matrix grayscale value, a pixel is recognized as a part of a worn area when its local mean is at least greater than the matrix grayscale value. The program does not work (A) with very high light exposures (E0 to F0). The same researcher would never read a slice with very high or low exposures (B). The combination of grayscale colors in (C) is the working area.

Test-picture, Accuracy, and Precision

The effects of the picture corrections made to enhance the readability of the pictures on the software's ability to detect differences in contrast were surveyed. A test dedicated to define the minimum contrast necessary to perceive the difference between whole matrix and a reabsorbed area was set up. The minimum contrast is defined as the smallest difference in the grayscale necessary to distinguish a pixel of a reabsorbed area from the surroundings belonging to the matrix. The analysis was performed for those brightness conditions estimated to be in the range useful for common reading by means of a test picture (Figure 3), including a gradient made of discrete combinations of gray levels for the estimated pixel and the surroundings. In the test picture the gray levels cover the range from HFFFFFF (white) to H000000 (black). This picture entered the first step of the picture scanning and the resulting set of detectable combinations of gray levels of reabsorbed and nonreabsorbed areas was ascertained. This set was defined as the working area and plotted in green in Fig. 3.

The maximum accuracy error was determined by scanning pictures containing geometrical figures of known dimension. Adobe Photoshop® was used to draw ellipses and polygons using combinations of gray levels included in the working area and for the background. Two orders of magnitude were considered: pictures whose dimensions were less or equal to the grid of the first step (7×7 pixels) and those extremely large compared to this grid. The maximum accuracy error was calculated in percentage as the difference be-

Table I. Comparison between the coefficients of variation obtained with the proposed software and with manual drawing using UTHSCSA image analysis software.

Our software				UTHSCSA image analysis software			
Osteologic BioCoated							
CV_{intra}			CV_{inter}	CV_{intra}			CV_{inter}
Invest. 1	Invest. 2	Invest. 3	3.9±1.5	Invest. 1	Invest. 2	Invest. 3	20.53±0.7
4.4±0.8	3.6±1.2	3.6±1.3		10.0±2.7	11.1±2.3	11.2±3.5	
Dentine							
CV_{intra}			CV_{inter}	CV_{intra}			CV_{inter}
Invest. 1	Invest. 2	Invest. 3	5.7±2.3	Invest. 1	Invest. 2	Invest. 3	10.7±4.3
4.3±1.9	4.8±1.0	7.8±2.5		8.0±2.2	9.4±4.2	7.9±2.5	
Bone slices							
CV_{intra}			CV_{inter}	CV_{intra}			CV_{inter}
Invest. 1	Invest. 2	Invest. 3	4.9±3.3	Invest. 1	Invest. 2	Invest. 3	9.6±3.2
4.1±1.7	4.6±1.9	6.4±1.7		7.3±2.5	8.4±3.2	7.4±1.9	

tween the average of the measured values and the true value. The precision was determined as intra-observer and inter-individual coefficients of variation (CV_{inter} and CV_{intra}). Three independent observers scanned on three different days the same set of five pictures of slices properly treated. In order to compare the results, in terms of accuracy, precision, and time, of our software with the current gold standard,[3,6,9,16] we repeated the tests using the UTHSCSA image analysis software available from the internet from maxrad6.uthscsa.edu (developed by Willcox and coworkers at the University of Texas Health Science Center at San Antonio, Texas). The CV_{inter} and Cv_{intra} obtained with our software or with the UTHSCSA were compared by paired Student's *t*-test.

Reliability Test

To evaluate the reliability of the method we studied the OCs' activity in ten healthy premenopausal women (mean age 33±7 years). OCs were generated by peripheral blood mononuclear cells (PBMCs) as previously described.[3] Briefly, PBMCs were obtained with the Ficoll-Paque method from 40 ml peripheral blood in lithium heparin. All cultures were performed in triplicate in 16-well plates BD BioCoat™ Osteologic™ Bone Cell Culture System (Becton Dickinson and Co. 4×10^5 cell/well) or on dentine slices (Pantec, 2×10^6 cell/well) using alpha minimal essential medium (α-MEM: Gibco) supplemented with 10% fetal bovine serum (FBS), benzyl penicillin (100 IU/ml), and streptomycin (100 μg/ml) (called "complete medium"), or complete medium plus M-CSF (25 ng/ml) and RANKL (30 ng/ml). RPMI (Gibco) was used for cell isolation. All cultures were maintained at 37°C in a humidified 5% CO_2 atmosphere. Cells were fed every 3 days. On the 21st day, they were fixed and stained for tartrate resistant acid phosphatase (TRAP) (Acid Phosphatase, Leukocytestaining kit, Sigma Diagnostics) and stained with an immuno technique to express the vitronectin receptor (VNR) (Becton Dickinson & Co.). OCs were recognized as TRAP+ and VNR+ multinucleated cells (>3 nuclei) according to the literature,[3,17] and were counted in each well. In order to avoid possible bias, the count was blind to culture condition and OCs were always identified by the same operator, and the mean per subject for 3 wells with and without M-CSF and RANKL was calculated. In order to evaluate OCs activity, cells were removed from the wells with 14% sodium hypochlorite after the count and a Nikon Coolpix™ digital camera attached to an inverted research microscope was used to photograph the entire surface of each well. Lacunar resorption was determined by examining each micrograph with our software or with the UTHSCSA software. For each well, four pictures at 20× magnification were taken. The operators were familiar with the use of UTHSCSA software, while they were novices in the use of our software.

RESULTS

Figure 3 shows the working area inside those range commonly used to picture fields of interest. Here is shown how discrete combinations of gray levels for the background and for the brightness of a single pixel are recognized by the first step of the picture scanning after the picture corrections to enhance its readability. The gray parts of the picture represent those combinations recognized. Those parts sketched, including the picture oblique, represent those combinations where the software is not able to distinguish the inquired pixel from the surroundings. This happens with brightness combinations close to the extremes and when the worn area and the matrix have the same gray level.

Our scanning procedure evaluates a pixel with respect to its background by means of the calculation of the mean on a grid of pixels, thus, it tries to emulate human vision. The method underlying the procedure implies the accuracy error to range from 0 to 100% in processing pictures, includ-

ing figures whose magnitude is minor or equal to the 7×7 pixels first step grid dimension. In fact, the operator is instructed to sample the threshold in a uniform area so that the pixels included in the 7×7 grid have basically a gray level characteristic similar to worn areas. This means that a single pixel randomly located on the picture, even though its gray level may be greater than the threshold, will not be recognized if it is surrounded by a grid of pixels such that the mean on the 7×7 grid is lower than the threshold. The extreme variability of the measurement accuracy for these small features is related to the chosen threshold and to the variable combinations of gray levels that contribute to determining the local mean brightness relative to the considered pixel $[M1(x,y)]$. As a consequence, inside the previously defined working area, we consider the minimum worn area detectable to be a resorption void of 7×7 pixels. It represents 0.0064% of the entire field of interest evaluated within a picture. Its absolute dimensions depend on the adopted magnification. Magnification of $10\times$ is considered to correspond to the presence of a single resorption void of approximately 66 μm^2. This void represents roughly less than the 1% of the surface occupied by a mature osteoclast. Inside the working area, the maximum accuracy error for pictures including geometrical features larger than the first grid is 0.16%. Low magnification and low picture resolution can invalidate the measurements. Results are guaranteed with pictures taken at $4\times$ or greater magnification and with at least a 2 megapixel picture resolution.

Coefficients of variation intra- and interobserver per culture system are shown in Table I. They were always found to be greater using manual drawing by means of the UTHSCSA image analysis software, but the difference was statistically significant only for the CV_{inter} calculated for the Osteologic Biocoated wells ($p=0.004$). Our results on accuracy and precision of manual drawing could even be overestimated considering that the area of the picture to be analyzed could become quite large in order to get usable results.

With respect to the reliability test, the number of OCs was significantly higher in a stimulated than in an unstimulated condition, OCs were able to reabsorb substrate only in a stimulated condition (Figure 4). The results obtained with the two techniques were not statistically different. The time required to analyze these pictures was, however, significantly different; on the average, 3 to 5 min are required for the complete analysis of a picture with our software, compared to the 10 to 15 min required with the standard procedure.

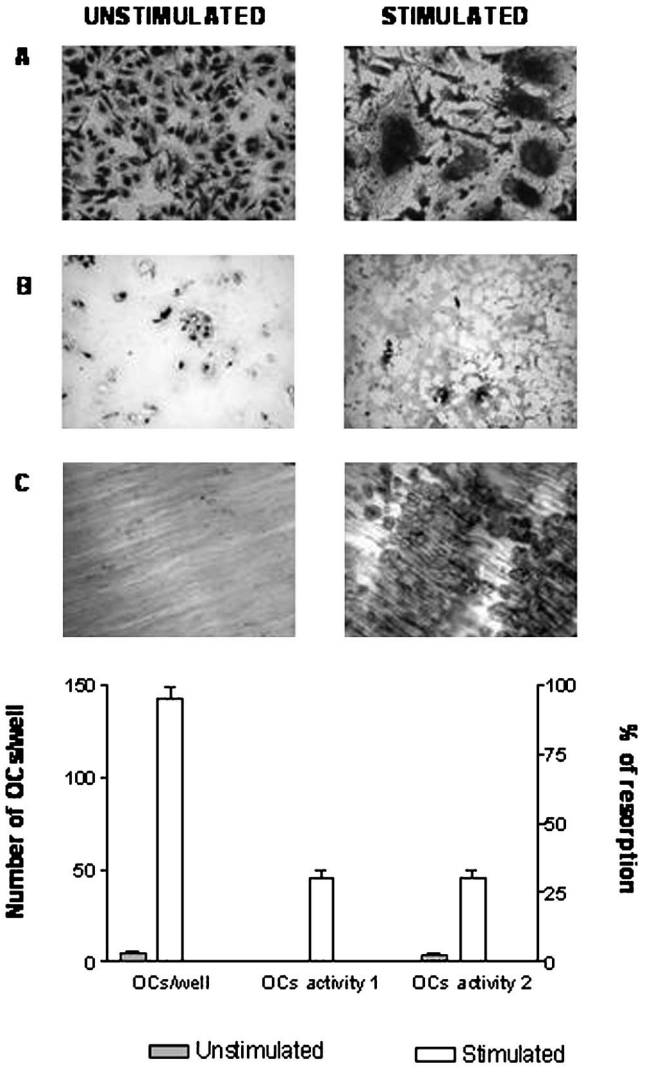

Figure 4. Osteoclast formation and activity under unstimulated and stimulated conditions. TRAP staining ($10\times$) of cultures of PBMC from healthy premenopausal women [unstimulated panel (a) left and stimulated panel (a)right]. Photographs of the hydroxyapatite matrix [panels (b)] and of the dentine slices [panels (d)] reabsorbed by the OCs. Histogram shows the number of OCs and the percentage of hydroxyapatite matrix reabsorbed, under unstimulated and stimulated conditions, in PBMC cultures. The OC activity was measured by means of our software (OC activity 1) or by means of UTHSCSA image analysis software (OC activity 2). The bars show the mean and standard deviation.

DISCUSSION

Handiness

Considering that a transmitted light microscope as well as a digital or conventional camera connected with an adapter to the microscope is a prerequisite for every bone research facility, we developed a semiautomated software technique targeted to assess osteoclast activity. This user-friendly tool does not require any additional frame grabber, thus improving its ease of use and reducing cost. Facilities can be vacated as soon as the photo sessions are concluded. Pictures analysis can be postponed and carried out on any standard computer not necessarily connected with the microscope. The link with an electronic datasheet ready for statistical analysis of data improves the handiness of this method.

Novelty

Software-based image analysis system and analysis of pictures on a pixel-by-pixel basis having defined threshold limits for the detection of peculiar features are not revolutionary innovations. The novelty lies in the development of a fast, dedicated tool for bone researchers and their user-friendly interaction with the software; the algorithm applies the researcher's real-time decisions. The architecture of the scanning procedure tries to emulate human vision weighting a

Table II. Comparison between the proposed software and other methods for the analysis of pit formation assays.

	Our software	UTHSCSA	B&D	Stereo mapping	Reflected light
Substrates systems required[a]	CPF, D, B	CPF, D, B	CPF	D, B	CPF, D, B
	Software	Software	Mycrost analyzer	Stereo microscope	Reflected light
Data collection	Automatic	Automatic	Automatic	Manual	Manual
Pit selection	Semi-automatic	Manual drawing	Automatic	Manual drawing	Manual drawing
Image analyzed	2D	2D	2D	3D	2D
Artifact exclusion	Yes	Yes	No	Yes	Yes
CV intra-observer	3.6%–7.8%	7.3%–11.2%	-	-	-
CV inter-observer	3.9%–5.7%	9.6%–20.5%	-	-	-

Calcium phosphate films (CPF), dentine (D), bone slices (B).

[a]Other than common research microscope with a digital camera and a personal computer.

pixel with respect to its background by means of the calculation of the mean on a grid of pixels. The operator is requested only to control the effect of the software's routine calculations, comparing the real-time developing images with the underlying original. By adjusting the thresholds the operator has the power to alter the result of the routine calculations until satisfied of the accuracy of the image.

Corrections carried out loading the picture improve its readability, enhancing the discrepancy between the pristine matrix pattern and the reabsorbed areas. The same corrections slightly reduce the software's ability to recognize as different some combinations of grayscale. These restrictions can be found in combinations of gray levels corresponding to conditions of slight overexposure or underexposure, but detection is guaranteed inside the commonly used visible range for slice reading. The scanning procedure allows singling out the worn areas and at the same time ignoring those small spots the operator recognizes as artifacts. The same lower limit of the architecture of our scanning procedure enables our software to cut off small artifacts. The dimensions of the first step grid are at any suggested magnification negligible with respect to the dimension of a mature osteoclast. This means that an isolated void of that dimension is not attributable to the osteoclast activity; rather, it is presumed to be to a matrix artifact. The algorithm underlying the second and third steps of the picture scanning allows the operator to refine the congruency of the edge of areas recognized as worn until a reasonable accuracy is obtained.

The main idea behind the development of our software is to allow the researcher to drive and verify the computer's choices and to eventually intercept artifactual results. Totally automated devices may have problems in recognizing adulterated parts of the slices, thereby overestimating the reabsorbed percentage. Examples are the slice edges or matrix damages due to culture seeding. With our technique the operator first chooses appropriate fields of view taking pictures where a meaningful analysis can be performed, and then erases macroscopic corruptions inside a field of interest. Ambiguous inferences are thus skipped.

Comparison with Other Methods

The intra- and interoperator coefficients of variation have shown that the precision of the software described here is admissible, and superior to that obtained by manual drawing using the UTHSCSA image analysis software. This difference is certainly not attributed to any malfunction of the latter software, rather to the duration of the manual drawing necessary for each picture, i.e., to the generally high number of reabsorbed areas per picture and to the researcher's ability to sustain concentration for the required spans in numerous photo sessions. In the present work we do not directly compare our methods with B&D instruments (Microst Image Analyzer), because we find it mandatory to control the image processing system in order to avoid biasing the results with artifacts.

Cell Cultures

Information on the cells' activity under specific metabolic conditions can be deduced from the results obtained by means of our algorithm. The resorption percentage can be considered as an image of the total aggressiveness of the cultured cells, and the number and the dimension of the single areas give an idea of the activity of each single cell. The two-color coding relative to the resorption percentage and to each single area dimension provides fast and intuitive results. The numerical results are automatically displayed in a database ready for statistics, making the analysis fast and tidy. The experiments performed in which proosteoclastogenic cytokines are added into cultures of PBMCs confirm that our software is able to discriminate different cell

culture conditions, and in so doing, it works faster than UTHSCSA software.

Shortcomings

The most striking limitation of our method certainly lies in its restriction to analysis of bidimensional images. Variable and not easily quantifiable accuracy errors on, e.g., dentine and bone slices, is the result. Even so, cell culture techniques are still preferred and their bidimensional images are analyzed by bone researchers.[3,6,7,10,15] For these applications, our software guarantees at least superior precision and repeatability of analysis compared to manual drawing. Table II shows a synoptic comparison between our software and other methods.

In conclusion, the combination of a common research microscope with a digital camera and our image analysis software proved to be a sufficient, easy-to-use, and relatively inexpensive tool to accurately determine osteoclasts' activity through assessment of their resorption capability, as demonstrated in this study. To spend a considerable amount of time evaluating by a repetitive procedure a very large number of pictures, as is usually necessary in a scientific study, can be frustrating and can cause imprecision. It is the present authors' opinion that the tool described here represents a reasonable compromise between control of the results and the time required to obtain them. However, the results of this bidimensional analysis are necessarily more accurate the thinner the matrix may be. Truly comparable results in bone research could enhance the understanding of how the resorption activity of either human or animal osteoclast may be modified by the action of bioactive agents or pharmaceutical agents.

ACKNOWLEDGMENTS

The authors are grateful to T. R. Arnett, who kindly provided the bone slice pictures, and to I. Roato, who kindly provided the dentine slice pictures for the software development. S.Z.M.B. and P.D'A. were supported by a grant from MIUR (COFIN 2003).

REFERENCES

[1] G. C. Nicholson, M. Malakellis, F. M. Collier, P. U. Cameron, W. R. Holloway, T. J. Gough, C. Gregorio-King, M. A. Kirkland, and D. E. Myers, "Induction of osteoclasts from CD14-positive human peripheral blood mononuclear cells by receptor activator of nuclear factor kappaB ligand (RANKL)", Clin. Sci. (Colch) **99**, 133 (2000).

[2] V. Shalhoub, G. Elliott, L. Chiu, R. Manoukian, M. Kelley, N. Hawkins, E. Davy, G. Shimamoto, J. Beck, S. A. Kaufman, G. Van, S. Scully, M. Qi, M. Grisanti, C. Dunstan, W. J. Boyle, and D. L. Lacey, "Characterization of osteoclast precursors in human blood", Br. J. Haematol. **111**, 501 (2000).

[3] P. D'Amelio, A. Grimaldi, G. P. Pescarmona, C. Tamone, I. Roato, and G. Isaia, "Spontaneous osteoclast formation from peripheral blood mononuclear cells in postmenopausal osteoporosis", FASEB J. **19**, 410 (2005).

[4] M. Jevon, T. Hirayama, M. A. Brown, J. A. Wass, A. Sabokbar, S. Ostelere, and N. A. Athenasou, "Osteoclast formation from circulating precursors in osteoporosis", Scand. J. Rheumatol. **32**, 95 (2003).

[5] G. D. Roodman and J. J. Windle, "Paget disease of bone", J. Clin. Invest. **115**, 200 (2005).

[6] S. Colucci, G. Brunetti, R. Rizzi, A. Zonno, G. Mori, G. Colaianni, D. Del Prete, R. Faccio, A. Liso, S. Capalbo, V. Liso, A. Zallone, and M. Grano, "T cells support osteoclastogenesis in an in vitro model derived from human multiple myeloma bone disease: the role of the OPG/TRAIL interaction", Blood **104**, 3722 (2004).

[7] I. Roato, M. Grano, G. Brunetti, S. Colucci, A. Mussa, O. Bertetto, and R. Ferracini, "Mechanisms of spontaneous osteoclastogenesis in cancer with bone involvement", FASEB J. **19**, 228 (2005).

[8] A. Sabokbar, R. Pandey, and N. A. Athanasou, "The effect of particle size and electrical charge on macrophage-osteoclast differentiation and bone resorption", J. Mater. Sci.: Mater. Med. **14**, 731 (2003).

[9] T. R. Arnett, D. C. Gibbons, J. C. Utting, I. R. Orriss, A. Hoebertz, M. Rosendaal, and S. Meghji, "Hypoxia is a major stimulator of osteoclast formation and bone resorption", J. Cell Physiol. **196**, 2 (2003).

[10] D. W. Dempster, C. E. Hughes-Begos, K. Plavetic-Chee, A. Brandao-Burch, F. Cosman, J. Nieves, S. Neubort, S. S. Lu, A. Iida-Klein, T. Arnett, and R. Lindsay, "Normal human osteoclasts formed from peripheral blood monocytes express PTH type 1 receptors and are stimulated by PTH in the absence of osteoblasts", J. Cell. Biochem. **95**, 139 (2005).

[11] I. E. Adamopoulos, A. Sabokbar, B. P. Wordsworth, A. Carr, D. J. Ferguson, and N. A. Athanasou, "Synovial fluid macrophages are capable of osteoclast formation and resorption", J. Pathol. **208**, 35 (2006).

[12] I. E. Adamopoulos, L. Danks, I. Itonaga, R. M. Locklin, A. Sabokbar, D. J. Ferguson, and N. A. Athanasou, "Stimulation of osteoclast formation by inflammatory synovial fluid", Virchows Arch. **449**, 69 (2006).

[13] B. J. Varghese, K. Aoki, H. Shimokawa, K. Ohya, and Y. Takagi, "Bovine deciduous dentine is more susceptible to osteoclastic resorption than permanent dentine: results of quantitative analyses", J. Bone Miner. Metab. **24**, 248 (2006).

[14] H. M. Massey and A. M. Flanagan, "Human osteoclasts derive from CD14-positive monocytes", Br. J. Haematol. **106**, 167 (1999).

[15] G. L. Bohnhoff, "Setting up proper illumination on your microscope", Am. J. Med. Technol. **45**, 650 (1979).

[16] G. Brunetti, S. Colucci, P. Pignataro, M. Coricciati, G. Mori, N. Cirulli, A. Zallone, F. R. Grassi, and M. Grano, "T cells support osteoclastogenesis in an in vitro model derived from human periodontitis patients", J. Periodontol. **76**, 1675 (2005).

[17] C. Shih and G. W. Bernard, "Peripheral blood mononuclear cells develop into multinucleated osteoclasts in tissue culture", Anat. Rec. **245**, 41 (1996).